# UC San Diego
## UC San Diego Electronic Theses and Dissertations

**Title**
Viral Vector Design and Lensless Imaging for Neural Tracing

**Permalink**
https://escholarship.org/uc/item/8cc2819p

**Author**
Zhang, Shuyang

**Publication Date**
2021

Peer reviewed|Thesis/dissertation

UNIVERSITY OF CALIFORNIA SAN DIEGO


Viral Vector Design and Lensless Imaging for Neural Tracing


A Thesis submitted in partial satisfaction of the
requirements for the degree Master of Science


in

Bioengineering


by


Shuyang Zhang


Committee in charge:

       Professor Todd Coleman, Chair
       Professor Lingyan Shi
       Professor Bruce Wheeler


2021

The Thesis of Shuyang Zhang is approved, and it is acceptable in quality and form for publication on microfilm and electronically.

University of California San Diego

2021

DEDICATION

To my grandparents

Who raised me and took care of me

My deepest gratitude

TABLE OF CONTENTS

LIST OF FIGURES

## ACKNOWLEDGEMENTS

I would like to acknowledge Professor Todd Coleman for allowing me to work under his lab as a master's student. Without his support and insights, I would not have this wonderful research opportunity.

I would like to acknowledge Dr. Phillip Kyriakakis for his invaluable mentorship and guidance throughout my undergraduate and graduate career. Thank you for being patient with my mistakes and pointing me in the right direction.

I would like to extend a special thanks to the past and present lab members for their kind help along this journey.

I would also like to extend a special thanks to my family for supporting me and trusting me throughout my life.

Chapter 2 and Chapter 3 are co-authored with Kyriakakis, Phillip, and Coleman, Todd P. The thesis author was the primary author of this chapter.

ABSTRACT OF THE THESIS


Viral Vector Construction and Lensless Imaging for Neural Tracing


by


Shuyang Zhang


Master of Science in Bioengineering


University of California San Diego, 2021


Professor Todd Coleman, Chair

Neuronal tracing methods are essential tools to understand the fundamental architecture of the neural circuits and their connection to the overall functional behavior of the brain. Various viral vectors have been developed to achieve cell-type specific and directional specific labeling of the neuronal connections. The incorporation of the viral tracers with optogenetics techniques can further provide precise control over the viral propagation. Herein, a novel approach to guide

the infectious pattern of the Rabies Virus (RV) retrograde tracer with light is described. The key concept is to use Baculovirus (BV) as a helper virus to deliver all the functional components prior to the rabies infection. These functional components include the optogenetic tool parts, a fluorescent CRE reporter to mark RV infected cells, and other genes necessary for RV spread. GoldenGate DNA assembly method was used to efficiently construct three large BV expression cassettes in bacteria plasmids that can be transposed into the baculovirus genome in a single TN7 transposon recombination step. The actual imaging of BV and RV infected cells and stimulation of optogenetics tools for the spread of RV can be achieved with CMOS sensor and OLED display panels. By integrating these commercially available electronics with proper microcontrollers, a synchronized communication protocol for optogenetic stimulation, image capturing, and file transferring was established in a lensless imaging setup. The OLED and CMOS sensor's large field of view and low cost allows this tracing method to scale many orders of magnitude greater than using microscopy-based methods.

**CHAPTER 1: INTRODUCTION**

In the nervous system, the information transfer or signal propagation occurs through a complex neural circuit composed of millions of neurons in the mouse brain and billions of neurons in the human brain that makes around $10^{15}$ neural connections. The basic units of this massive network structure, individual neurons, can be split into three parts: the dendrites, the cell body/soma, and the axon. The connections between the neurons are located at synapses between the axon terminal of the presynaptic neuron and the dendrites of the postsynaptic neuron. These synaptic connections form specific neural pathways for the nervous system to efficiently communicate and achieve essential neural functions such as information processing and memory storage[1]. In order to understand the detailed relationship between neural pathways and their corresponding functions, neurons are labeled, and their connections to other neurons are observed through the implementation of the neural tracing methods. By reconstructing the architecture of neural pathways, researchers can build empirical models to analyze the behavior of the nervous system and to determine the pathological cause of many psychiatric diseases[2]. As a result, the development and optimization of many kinds of neural tracing methods have been ongoing since the 1970s[3]. Today, the applications of neural tracing methods are capable of unveiling functional neuroanatomy with highly specific genetic labeling and with high spatial, temporal precision. However, the scalability of these systems to mapping many connections at once and the lack of automation greatly limit what can be labeled.

1.1 Neural Tracers

The central principle that most modern neural tracers use was introduced by Kristensen and Olsson in 1971[4,5]. They recognized that the molecular transporting mechanism along the axons of the nerve cells can also be used to carry chemical substances with cell-labeling

1

potentials[5]. This intrinsic cellular cargo movement, also called axonal flow, became the mainstream approach for tracers to travel within neurons. Traditionally, isotope-labeled amino acids were used as tracing units to label structural details of the central nervous system[6,7]. However, these tracers relied on bulky autoradiographic instruments for detection[7]. Nowadays, the common neuron tracing methods utilize conventional light and/or microscopes to image neural tracer. Current tracing methods can be divided into conventional tracers and viral tracers depending on the substance and mechanism[6].

Conventional tracers are composed of chemical materials that can be detected by immunohistochemical techniques, or their intrinsic fluorescent properties. Some of the earliest methods of neural tracing rely on fluorescent transport substances, such as Evans Blue dye (EB), that are directly injected into neural sites[8]. However, since these substances can freely diffuse between cell membranes, they were soon replaced by fluorescently tagged beads that are specific to the neurons[8]. Upon engulfing by the neural cells through passive endocytosis at the injection sites, these beads are transported between cell soma and axon terminal through axonal flow[9]. During this process, motor proteins like kinesin or dynein bind to the cargo complex and drag it along the axon. Since this movement of the cellular cargo can be administered bi-directionally, anterograde and retrograde, neural tracers are categorized as one or the other or both. The retrograde tracers get transported from the axon towards the cell body or soma. Anterograde tracers get transported from soma toward the axon terminal[3]. One of the drawbacks of using fluorescent beads as the neural tracer is the inefficient uptake rate of the tracer elements by the neurons with the passive endocytosis process[8]. In order to overcome this inefficiency, conjugates such as horseradish peroxidase (HRP) or Cholera toxin subunit B (CTB) have been developed to take the advantage of binding to membrane bond carbohydrates which increase the uptake

through sugar mediated channels[8]. In the case of HRP-CTB, CTB binds to the GM1 ganglioside and gets transported into the cell through a special receptor which contributes to a higher uptake efficiency than the passive endocytosis of the native HRP[8]. The conventional tracers are also restricted in the range that they can be transported around the injection site due to active degradation and limited concentration of receptors on the synaptic junction[10]. As a result, staining long-range connections between the neurons can be difficult for these types of tracing methods. In addition, these tools are not genetically encoded on a viral vector or in the genomes of the neurons, making cell-type-specific labeling challenging.

Unlike previous methods, viral tracers such as herpes simplex virus (HSV), Adeno-Associated Virus (AAV), and RV efficiently enter neurons and travel anterogradely, retrogradely, or both. In addition, they can express reporter proteins with genetic/cell type specificity that can be imaged with light and electron microscopy or they can express tools such as opsins or DREADDS that can modulate the neural activity of the labeled cells[11, 12]. Depending on which viral tracer is used, the neuron labeling can be (1) static, only labeling neurons with initial contact, they can be (2) monosynaptic, labeling the first order of neurons that have a synaptic connection with the initial neuron, and they can be (3) polysynaptic, labeling multiple orders of synaptically connected neurons. The combination of viral tracers with programmable transgene expression systems such as Cre-LoxP makes the replication-competent neurotropic viruses ideal candidates for genetically controllable mapping of single synaptic connections[13]. Depending on the properties of the virus the tracers are derived from, there are in their interactions with the host genome, maximum genetic payload size, cellular transport, and transgene expression levels[6]. The maximum transgene payload size of each viral vector is mostly limited to the size of the native genome. For example, AAV can be packaged with around 5kb[14,]

of transgene, lentivirus can be packed with approximately 8kb of transgene[14], and RV can

package up to 7.5kb if rescued with the rabies glycoprotein and *L* gene in trans[15,16]. A large

packaging capacity allows the viral vector to contain more tools for labeling and controlling viral

tracers or could be used to deliver larger genes for gene therapy. While viral tracers can

efficiently deliver genes into cells, outside stimuli, such as light, can be used to achieve higher

specificity labeling or control of cellular activity and can be used to minimize toxicity of the

tracing tools.

## 1.2 Optogenetics

Optogenetics is a method to induce specific neuron behavior with light through

genetically introduced photoreceptors. Many different types of photoreceptor proteins have been

derived from plants, bacteria, and algae and modified to control cellular activities or target gene

expression[17,18]. These light-sensitive phytochromes possess useful and diverse functional

properties which can be integrated into various applications[19,20,21]. By bind to different

chromophores, the phytochrome protein can absorb light from numerous bandwidth ranging

from UV to NIR parts of the spectrum[18]. For example, some phytochromes are activated with red

light and are stable for hours in this activated state unless deactivated with far-red light[19]. Others

are responsive to green and red light[22] or UV/Violet and green[23]. The phytochrome protein

utilizes the tetrapyrrole chromophores such as phycocyanobilin (PCB), biliverdin (BV), or

phytochromobilin, which isomerizes upon absorbing a photon, leading to conformational

changes in the protein. Introduce Phytochrome B (PhyB), then talk about red and FR light.  to

convert between the red light absorption state (Pr) and far red light absorbing state (Pfr)[24]. Once

exposed to red light, chromophores activate the conformational change of phytochrome turning

Pr into Pfr form. In the Pfr form, phytochrome releases its COOH-terminal binding pocket which

4

allows the dimerization with a specific Phytochrome-Interacting Factor (PIF). This process is also reversible with far-red light that inactivates the Pfr phytochrome and causes the dissociation with the PIF protein. Since the binding between phytochrome and PIF proteins can be engineered to modulate downstream effects in the signaling pathways, phytochromes are often used as photo-responsive toggles to transmit light information into cellular signals in optogenetics applications[25].

The most studied and explored phytochromes for gene regulation is the Phytochrome protein B (PhyB) and its interacting factor PIF3. The fundamental setup of this system is to bind PhyB and its interacting factor PIF3 with DNA-binding Domains (DBD) and transActivation Domains (AD) respectively[26]. Under ambient conditions, DBD linked PhyB is in the Pr form which blocks its dimerization process with PIF3. Subsequently, it also blocks its binding with AD and inhibits downstream transcription. Upon red light activation, the fusion between PhyB and PIF3 proteins recruits AD to promote the expression of targeted genes. This process is also reversible with NIR light which dissociates the fusion complex and silencing the expression[26]. Another considerable feature of the PhyB phytochrome is its nucleus translocation property upon red light activation. This special feature makes it an ideal candidate to increase the DNA transcriptional efficiency in gene delivery. As shown in the Gomez *et al.* paper[27], PhyB/PIF system was integrated with the AAV genome to allow light-controlled nuclear translocalization of the viral vector. The study designed AAV vectors to express PIF and HeLa cells to produce PhyB. Since the PIF proteins are expressed on the capsid of the virus, the fusion between the PIF and red light-activated PhyB with translocational properties granted the viral particle a more efficient entry into the cellular nucleus which is considered as the rate-limiting step in the AAV transduction process[27]. In this thesis, the rabies viral vectors that have been recombinant for

neural tracing utilize this PhyB/PIF3 optogenetic switch system to regulate tracer activities within the neurons.

## 1.3 Hardware Setup for Optogenetics

As stated previously, the illumination systems that are applied in optogenetics can be fine-tuned based on different scenarios. Adjustable parameters for an optical system include: (1) the wavelength of the light source, (2) focal intensity, (3) spatial and temporal resolution, (4) power consumptions, and (5) the cost of the equipment itself. The commonly used light sources for optogenetics purposes are light-emitting diodes (LEDs) and lasers. Laser-based illumination sources can emit light at a specific wavelength with a high-intensity level (*e.g.* 100mW)[28]. When coupled with optical fibers, laser light sources can achieve precise optical activation of the neurons in specific intracranial locations. In contrast, LEDs are semiconductor devices that emit monochromatic light that is neither spatial nor spectral coherent. Nevertheless, with major developments over the past decade, current LEDs have relatively specific bandwidth and stable intensity over long periods of time[29]. On top of that, their relatively cheap price and broad-spectrum color options make LEDs the optimal illumination source for large-scale multi-channel stimulation[30]. Furthermore, because many optogenetics constructs are made to co-transcript target genes with fluorescent reporters to visualize and quantify the gene expression profile, compatible illumination devices often integrate functions for both photoreceptors activation and fluorophores excitation[28]. The miniature size of the LED devices also makes them highly compatible with emerging computational imaging methods like lensless imaging[31] which was one of the aspects of this project.

**CHAPTER 2: VIRAL TRACER PLASMIDS CONSTRUCTION**

2.1 Background on Retrograde Synaptic Labeling with Rabies Virus

Recombinant viral vectors engineered to express transgene proteins while retaining their self-replication ability are promising approaches for polysynaptic neural labeling within the nervous system. As one of the earliest viruses used for transneuronal tracing, rabies virus (RV) has been extensively applied in mapping long-range connections from the peripheral motor neurons to the neuron groups in the central nervous system because of its retrograde transferring property[32]. This property was exploited with the development of the RV variant derived from the Street Alabama, Dufferin (SADB19) strain with glycoprotein (*G* gene, or "G") deletion (SADΔG). The RV glycoprotein is expressed on the viral capsid and is necessary and sufficient to enable synaptic spreading from one neuron to another[33]. Since RV, like other enveloped viruses, relies on the interaction between the capsid-bound glycoprotein and the target cell's surface receptors to gain entry, the RVΔG becomes incapable of infecting and transducing neurons[33]. However, studies have shown that this functional loss can be rescued by expressing the G protein *in trans* and used to control the trans-synaptic spread of the RV[34]. Therefore, systems that use helper viruses (such as AAV or Lentivirus) or transgenic animals to complement the RV glycoprotein and/or its cognate receptor, TVA, into desired neuron-types have been developed to achieve selective infection of the ΔG mutant for cell-type-specific labeling[34].

Similar to other replication-component viral vectors, one of the major impediments of integrating this ΔG variant of the RV with long-term imaging tools is the cytotoxicity in the neurons of interest. As observed from time-lapse studies, neurons infected with RVΔG show structural degradation and cell death within two weeks[16]. The neurons killed by RV infection release RV into the extracellular environment, producing non-synaptic/nonspecific spreading of

RV labeling neurons that are not in fact synaptically connected to the neurons being studied[6]. In addition, this restricts the experimental time for tracing and causes effects on the anatomy and physiology of the nervous system being studied. Because of this limitation, tracing experiments using the replication-component RV or ΔG RV are often restricted with cursory observation windows[3].

Mutant RV vectors with deletion of both *G* and *L* genes (ΔGL) were introduced by Soumya Chatterjee *et al.* to minimize the cellular toxicity and allow for long-term neural labeling[35]. Compared to the traditional ΔG version of the RV tracing vector, this specific nontoxic variant tuned down the viral genome replication rate by additionally knocking out the viral polymerase, the *L* gene, that catalyzing the transcription of viral mRNA and replication of viral genome[36]. While non-toxic, Chatterjee *et al.* showed that neurons infected with the ΔGL RV encoding enhanced green fluorescent protein (EGFP) exhibited a minimum level of transgene expression for fluorescent detection[35]. However, when the RVΔGL includes a Cre recombinase, it is capable of inducing high levels of GFP expression in transgenic mice containing a Cre-dependent GFP reporter[35]. This resulted in a long-term observation window with cell postinfection survivability. While this important work showed that the non-toxic RV strain could infect neurons and label them effectively, the large size of the *L* gene made it impractical to rescue RV's ability to spread. It effectively became a non-toxic neuron labeling vector rather than a system to map synaptic connections. In order to utilize the nontoxic ΔGL-Cre RV as a neural tracer, an expression system to supply the glycoprotein, the glycoprotein receptor (TVA), and the *L* protein is required[35]. In this work, helper viral vectors that integrate the production of all of the complementary proteins were constructed. These vectors contain a PhyB/PIF3 optogenetic tool for optical control of genes[19], and a novel Cre-dependent reporter system, all in one BV vector, to

trace neuronal connections with the high-resolution control of light.

## 2.2 Baculovirus Expression Vector Design and Construction

Using traditional methods, packaging all the functional elements is not a simple task. The combination of gene sizes (*L* gene (6.7kb), TVA+*G* gene (3.4kb), PhyB/PIF3 gene switch (6.7kb),  Cre dependent reporter (4.1kb)) and other gene regulatory systems for long term expression (total 26.5kb) ) far exceeds the transgene limit of commonly used viral vectors (AAV virus (5kb) and lentivirus (8kb)). Therefore, the baculovirus vector with an effective transgene size of over 100kb[37] was chosen to deliver the necessary components. Furthermore, the baculovirus infection has very low cytotoxicity in mammalian cells, even at high Multiplicity of Infections (MOI)[38] which makes it an ideal helper virus for the nontoxic RVΔGL. In this section, I will first describe the genetic circuitry that allows the PhyB/PIF3 gene switch to control the expression of the *L* gene. Then, I will illustrate the overall schematic and interaction between the baculovirus and the non-toxic RV tracer.

### 2.2.1 Molecular Mechanisms of Gene Switches in the Viral Vectors

To enable non-toxic and light controllable neuronal tracing, the baculovirus helper virus is designed with two gene control systems to interact with ΔGL-Cre rabies vector: (1) the PhyB optogenetic system that regulates the expression of the *L* gene (*i.e.* RV spreading) (**Figure 1A**), and (2) the Cre-dependent reporter system which will mark neurons that can be traced and will label the RV infectious pathways within the neural circuit (**Figure 1B**). In the optogenetic system, the PhyB photoreceptor is linked with Gal4 DNA Binding Domain (Gal4 DBD) and interacts with the PIF3 protein linked with the Activation Domain (AD) in a red/far-red dependent manner, activating genes after the Gal4 Upstream Activation Sequence (UAS) promoter. When the PhyB is inactive (Pr), it is bound to the promoter, but not to PIF3-AD, *L*

gene expression is off and double deletion RV will not replicate or spread. Once PhyB is activated (Pfr) by red light and forms a complex with PIF3-AD, the *L* gene expression is induced and the RVΔGL will be able to replicate and spread. The Cre-dependent reporter system contains the target reporter genes flanked by specific sequences, LoxP sites, in a Double-floxed Inverted Orientation (DIO). When the neuron of interest is only infected with BV, the upstream promoter will express a target gene sequence (Nuclear Localized GFP, NLS-GFP). Then, when the neuron of interest is infected with RVΔGL-Cre, the presence of Cre recombinase will result in permanently inverting the gene orientation of the reporter cassette. After this inversion, the mScarlet-CAAX[39] fluorophore will be expressed instead of NLS-GFP: switching from fluorescent nuclear green expression (for targeting/aiming red light to specific neurons/nuclei) to the RV infected neurons containing a red fluorescent membrane label, which will mark the entire neuron with high contrast. Through this novel Cre-dependent reporter system, the transneuronal propagations of the RV can be labeled and differentiated from neurons only infected with the helper virus.
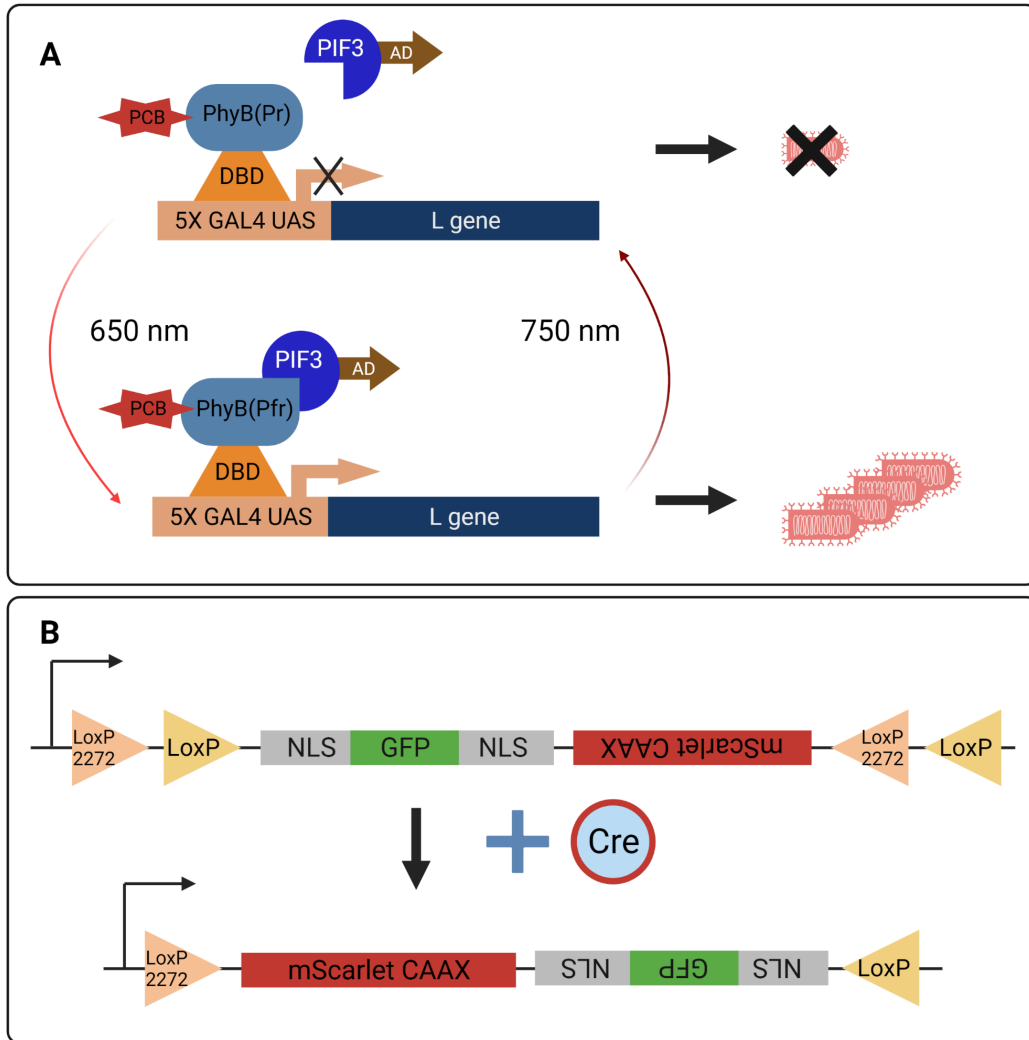
**Figure 1: Gene Switches for expressions of L protein and fluorescent reporters.**

**A)** The PhyB photoreceptor is bound to the Gal4 UAS promoter through the DNA Binding Domain (DBD) and its light-dependent interacting protein PIF3 is linked with gene Activation Domain (AD). In the dark, PhyB does not dimerize with PIF3-AD, leaving the *L* gene in the uninduced state. The lack of *L* gene expression limits RV replication. Upon absorbing the red light (~650 nm) by PCB chromophore+PhyB, PhyB changes to Pfr configuration and recruits the PIF3-AD complex, inducing the expression of the *L* gene. Once the *L* gene is induced, the RV genome is replicated and RV is produced and spreads to neurons synaptically connected to the neuron that was illuminated with red light. This process can be reversed or suppressed with far-red light (~750 nm).

**B)** The fluorescent Cre reporter is flanked with DIO LoxP sites. In the starting orientation, only the NLS-GFP sequence was transcribed and translated. After Cre recombination, the DNA orientation is permanently inverted and a mScarlet-CAAX reporter is expressed. Therefore, the outline of the neurons infected with ΔGL-Cre RV can be easily identified.

2.2.2 Using Baculovirus as Helper Virus for Rabies Neural Tracer

The baculovirus is designed to deliver four main functional components: the PhyB/PIF3 optogenetic switch for light inducible *L* gene expression, the *L* gene under the control of the Gal4 UAS, the TVA/G proteins for selective cell entry and spread, and the Cre-dependent fluorescent reporters. With these genetic parts combined, the light-controlled spread of the non-toxic RVΔGL-Cre for mapping the neuronal connections can be achieved (**Figure 2**). For *in vitro* and in brain slice experiments, the baculovirus will first infect neurons at a high MOI to infect as many neurons as possible, producing TVA/G proteins, the NLS-GFP reporters, and the PhyB/PIF3 optogenetic switch (**Figure 2A**). After that, RVΔGL-Cre is introduced into the neuron samples and can only infect cells previously infected with the BV that expresses the TVA receptor (**Figure 2B**). Once inside the neuron, Cre from inside the RVΔGL-Cre particle recombines with the Cre reporter switching the NLS-GFP expression to mScarlet-CAAX (red fluorescence on the membrane surface). Since the RVΔGL-Cre is replication-deficient in the absence of *L* gene expression, the viral load will remain non-toxic and unable to infect other neurons. Then using red light illumination, expression of *L* gene is induced through the PhyB/PIF3 optogenetic switch. By complementing the *L* gene with light, RV ΔGL-Cre replicates and spreads through retrograde synaptic connections. This process can then be repeated to label the next-order connections and can be parallelized to map multiple circuits at once. In addition, by regulating the *L* gene with light, toxic *L* gene expression can be transient and minimized compared to the wild-type RV, enabling mapping polysynaptic connections of neural circuits, while constraining the toxicity of the system to single cells.

**Figure 2: Schematic of using BV as a vector to allow selective neuron entry and pathway labeling of the RVΔGL-Cre strain.**

**A)** To express the tracing components in neurons, BV vectors carry most of the genetic circuitry. Upon initial BV infection, BV enters the cell through the native BV glycoprotein, GP64, as well as the VSV-G glycoprotein (to enhance infection efficiency). Once the baculovirus is transduced into the neuron, TVA+G proteins and NLS-GFP are expressed. Infecting BV infected neurons with RVΔGL-Cre by limited dilution or by injection into specific locations a "starter cell" or "starter cells" are selected for mapping. Neurons infected with RV ΔGL-Cre will recombine the Cre reporter, switching from NLS-GFP production to mScarlet-CAAX production.

**B)** Initially, the mScarlet-CAAX labeling will only appear in the neurons infected with both BV and RV ΔGL-Cre. Through a pulse of red light, the PhyB/PIF3 gene switch will induce *L* gene expressions. The resulting L protein catalyzes the RV ΔGL-Cre genome replication and spreads connected neurons previously infected with BV.

(BV = Baculovirus, G protein = Rabies Glycoprotein, GFP = Green Fluorescent Protein, TVA = Tumor Virus receptor A, and RV = Rabies Virus)
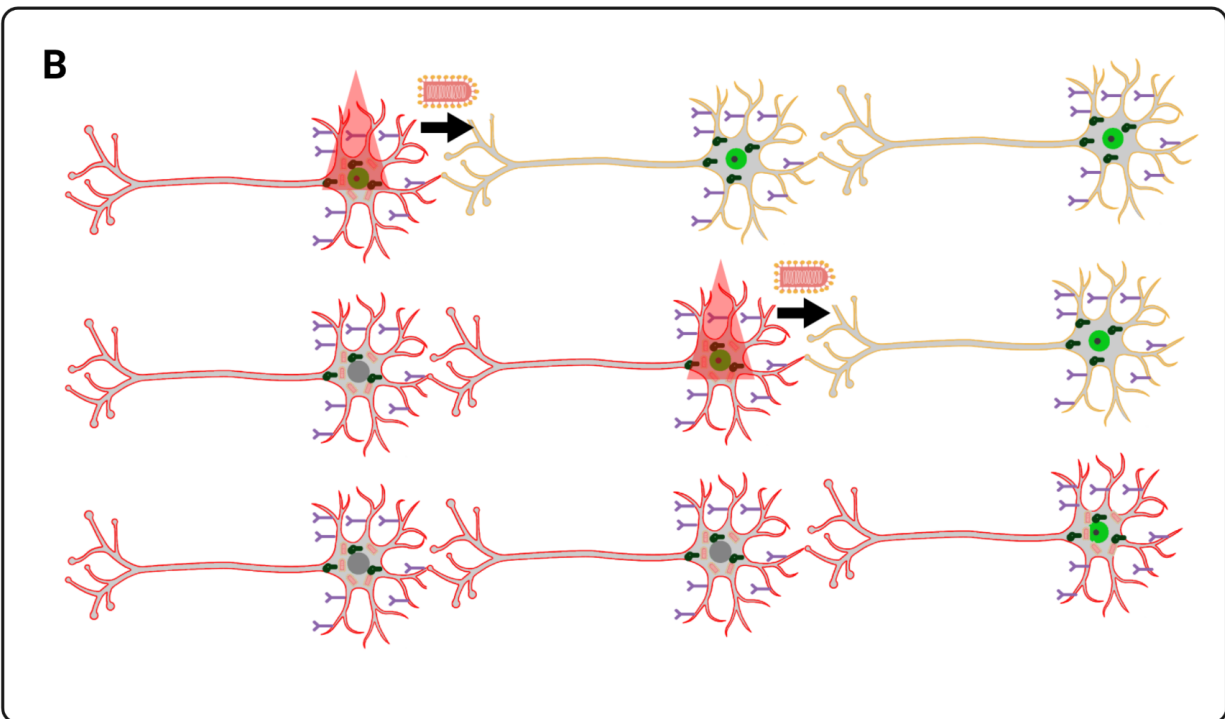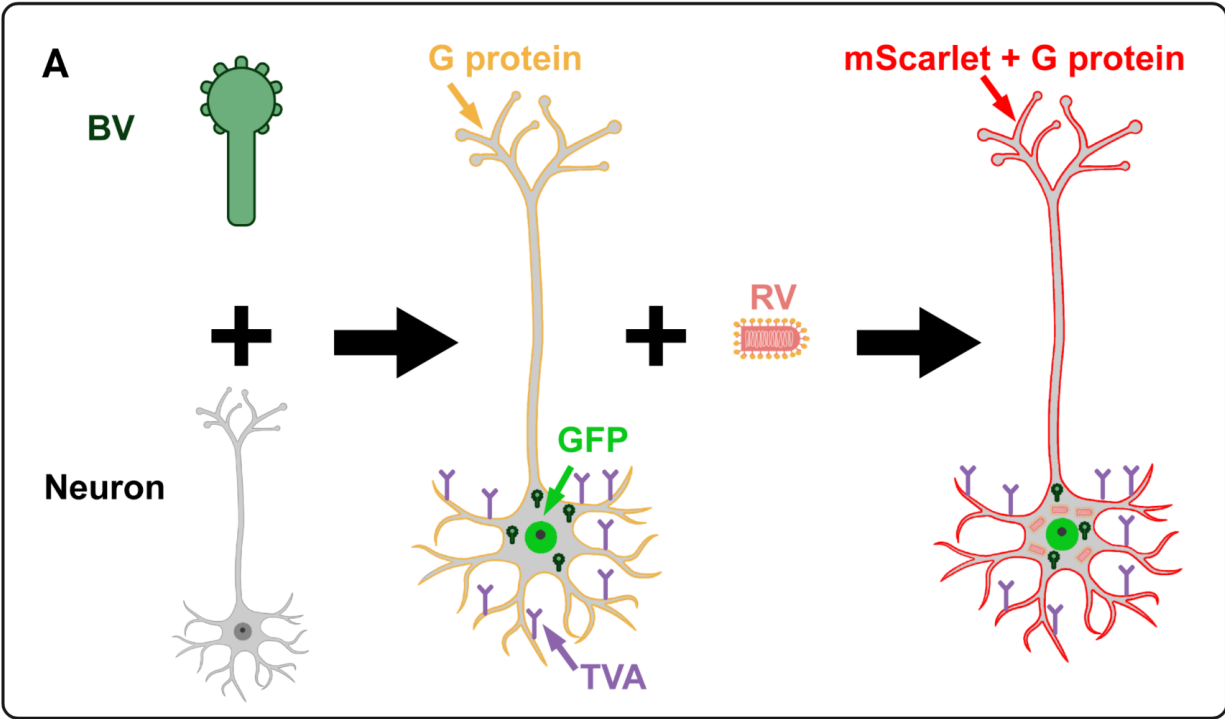
2.2.3 Baculovirus Expression Constructs

The Bac-to-Bac (Bacteria to Baculovirus) system allows the specific DNA to transfer from the bacterial donor plasmid into the baculovirus receiver vector, allowing efficient insertion of large constructs into the BV genome[40]. The overall mechanism of this technique works by transposition of a target DNA/gene flanked with Tn7 transposon elements sequences, Tn7L and Tn7R on a bacterial plasmid into the attnTn7 docking sites on the baculovirus shuttle vector in bacteria (also known as bacmid, essentially a very large plasmid or Bacterial Artificial Chromosome (BAC))[40]. This allows for the simpler insertion of genes into the BV genome and allows for easy clonal selection prior to virus production. In this work, I produced three resulting plasmids for inserting into the BV genome: the PhyB-Lgene (described in detail above and in **Figure 3A**), PhyB-destableLgene, and positive control construct. PhyB-destableL-gene (**Figure 3B**), is a variant of the PhyB-Lgene plasmid constructed to express a destabilized version of the *L* gene/protein when activated by light. By adding a PEST sequence (polypeptide sequence enriched in proline (P), glutamic acid (E), serine (S), and threonine (T)) in front of the *L* gene, the resulting L protein will be signaled for rapid intracellular breakdown and degradation[41]. This approach was taken because of the nature of the *L* gene/protein (a polymerase), only small quantities may be required for function. Since any genetic system is noisy, small amounts of the stable *L* gene expressed in the dark or from light scattering from a target activation region may induce unwanted RV ΔGL-Cre spreading, the destabilized version can provide tighter control of the spreading system. The positive control constructs constitutively expresses the *L* gene, leading to light independent spreading, ensuring that the RV ΔGL-Cre can be complemented by the BV system and can aid in the optimization of the optogenetic versions (**Figure 3C**).

**Figure 3: Gene maps for PhyB-Lgene, PhyB-destableLgene, and positive control constructs.**

**A)** The fully assembled PhyB-Lgene plasmid contained seven main functional groups: (1) the PhyB optical gene switch, (2) the fluorescent Cre reporter, (3) the TVA/G protein expression cassette, (4)the light-inducible L gene, (5) a bacterial selection marker for inserting the genes into the BV genome, (6) a bacterial selection marker for plasmid cloning, and (7) the Vesicular stomatitis virus glycoprotein (VSVG) for enhanced transduction into mammalian cells. The entire baculovirus expression cassette is flanked by Tn7 transposon sites for Tn7-mediated transposition into the bacmid vector. The size of the resulting plasmid is 29.4kb.

**B)** The fully assembled PhyB-destableLgene plasmid contained the same parts as the stable L-gene construct, except the *L* gene used was modified with the addition of a PEST sequence on the N-terminus.

**C)** The positive control plasmid contains the L gene under the control of the constitutive EF1a promoter instead of a light inducible promoter.

(CamR = Chloramphenicol Resistance, D4Z4C = insulator, EF1a = Eukaryotic translation elongation Factor 1 alpha 1, WPRE = Woodchuck hepatitis virus Post-transcriptional Response Element, BGH PA = Bovine Growth Hormone PolyA tail, Syn = Synapsin promoter, Rabb beta = Rabbit beta-globin PolyA tail, SV40 PA= Simian Vacuolating virus 40 PolyA tail, SpecR = Spectinomycin Resistance, KanR = Kanamycin Resistance)
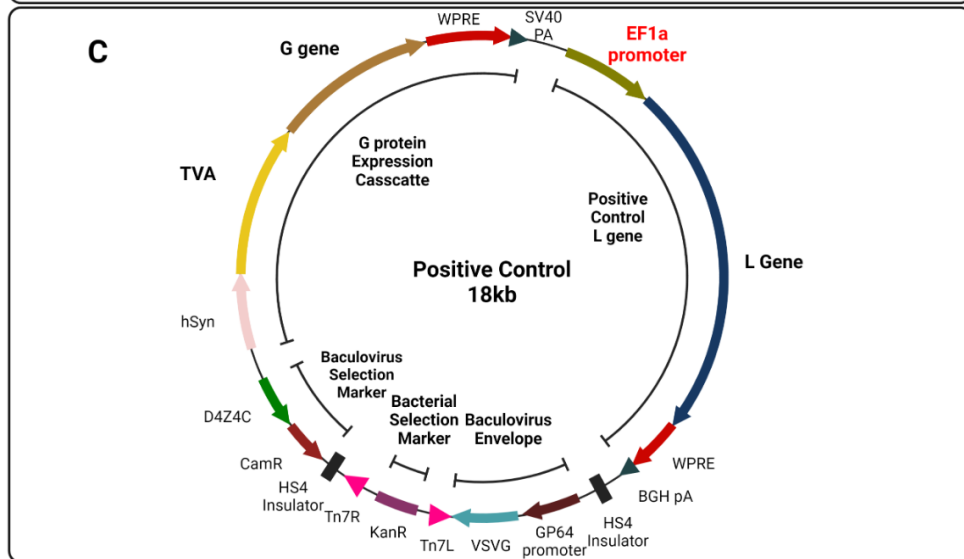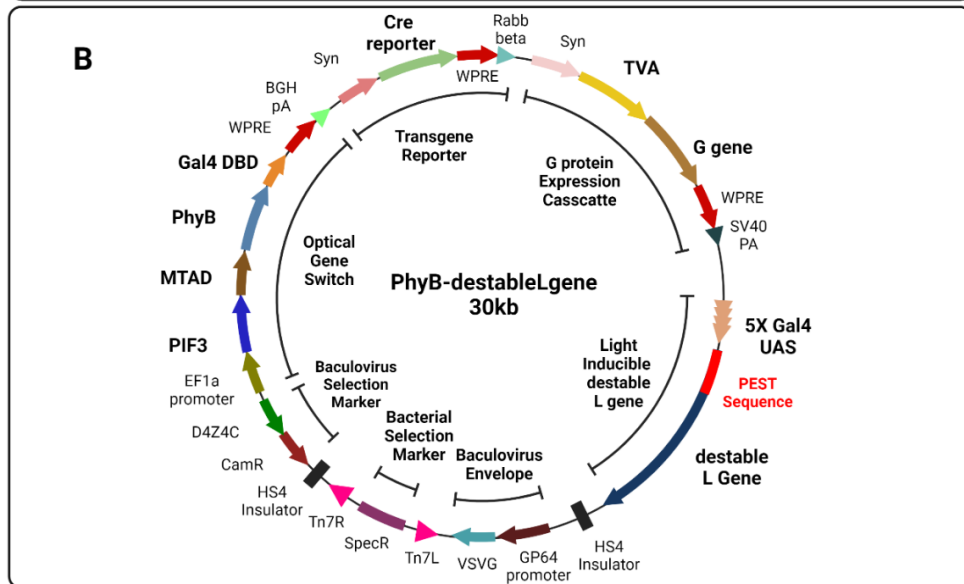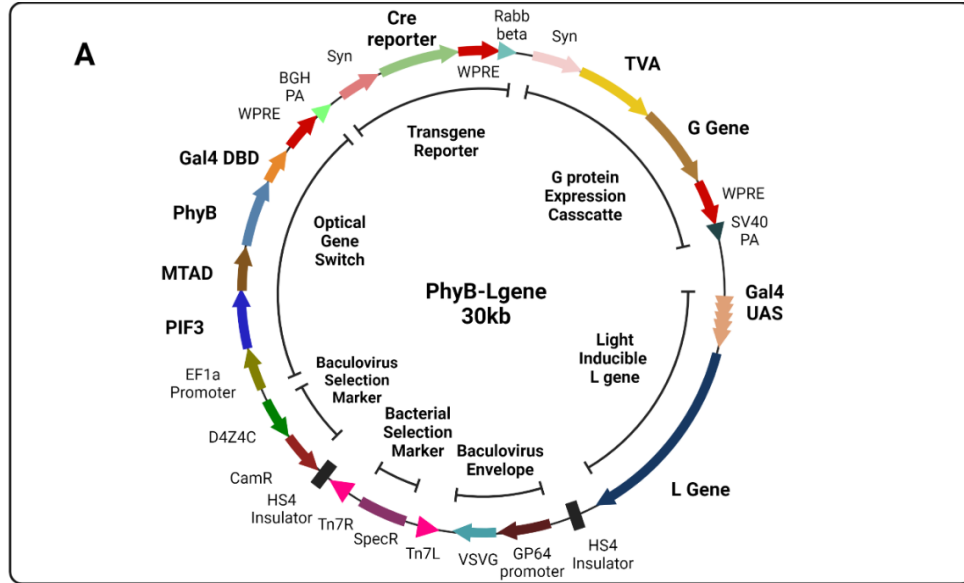
## 2.3 Materials and Methods

The workflow of DNA plasmid construction for this project is shown in **Figure 4**. The DNA sequence design was done using a Google Sheet template and with the open-source Multiplatform DNA editing software, A Plasmid Editor (APE). After designing the high-level construct in the Google Sheet, low-level parts were designed on the sequence level using APE, such that they could be assembled using a GoldenGate-based DNA[42] assembly method uLoop[43] into the final construct (detailed in section 2.3.1). Low-level parts are produced and combined with uLoop[43] and then transformed into *E. coli* to amplify them for sequence analysis and subsequent assembly into larger parts. To amplify the resulting DNA, the *E. coli* were grown and the DNA was extracted and purified by miniprep. The purified DNA is then sequenced or analyzed by restriction digestion prior to subsequent rounds of DNA assembly.
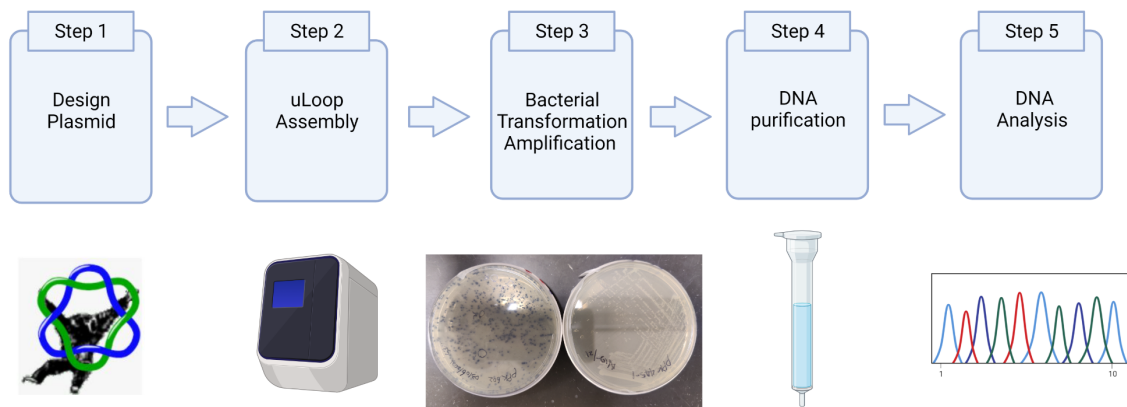


**Figure 4: Overall workflow of the plasmid construction.**

### 2.3.1 DNA Fabrication with uLoop Assembly

Construction of bacterial plasmids containing the expression cassettes for baculovirus vectors was done through the uLoop assembly method detailed in Bernado *et. al.*[43]. This Type IIS restriction enzyme-based DNA assembly method is capable of generating large constructs of DNA plasmids (~30kb) by recursive DNA assembly (**Figure 5**). In the uLoop method the Type

18

IIS restriction enzymes used are BsaI and SapI. Type IIS restriction enzymes like Bsa1 and Sap1 make DNA cuts at a specific distance away from their recognition sites, allowing cutting the DNA while removing the Type IIS site and generating customized hangover sites, essential properties for Golden Gate-based DNA assembly methods (**Figure 5A**). In uLoop, BsaI and Sap1 digestion sites are arranged in a manner, which is reversely oriented in odd (L1, L3, *etc.*) and even (L2, L4, *etc.*) levels[43]. To produce level 1 parts (L1), the basic gene elements are "domesticated" and then assembled into the odd receivers plasmids. This domestication process involves removing BsaI and SapI sites from the wild-type gene sequences to prevent cutting the parts during the assembly process. For large DNA elements such as the *L* gene, multiple mutations were required to achieve complete domestication. Thus instead of making silent mutations to remove these sites, the C-terminal part of the *L* gene was synthesized from scratch (IDT gBlock) using different codons. In the next step of uLoop, four L1 plasmids are assembled together into an even receiver plasmid to make a level 2, or L2 plasmid (**Figure 5C**)[43]. During this process, the SapI enzyme cleaves the parts out of L1 plasmids and removes the *lacZ* marker on the even receiver. Then, four compatible L1 parts/overhangs ligate to each other and form an L2 plasmid containing desired parts in a predetermined orientation (**Figure 5B**). This process is repeated for the assembly of L3 plasmids, using the BsaI restriction enzyme instead of Sap1. L4 plasmids can then be produced using the SapI enzyme again (**Figure 5C**). The even and odd receiver vectors are also tagged with two different antibiotic selection markers (KanR, for odd vectors; and SpecR, for even vectors) to select for the assembled DNA in *E. coli*. Additionally, the inclusion of the *lacZ* gene within the receiver vectors permits blue-white screening to differentiate the assembled plasmid products from the uncut receiver vectors. The detailed reagents and protocols used for the assembly were adopted from the Pollak *et al.* study.[43]

**Figure 5: uLoop assembly with LacZ implementation for blue-white selection.**

**A)** BsaI and SapI are the two Type IIS restriction enzymes used for uLoop assembly. Their corresponding recognition sites are labeled in blue for BsaI and red for SapI. The backbone of the uLoop assembly uses the property that Type IIS enzymes cut outside the recognition sequence to generate customized single-stranded overhangs for position-specific DNA part assembly. The inverted placement of these restriction sites allows the enzyme to effectively cut out the *lacZ* gene from the backbone plasmid and leave overhangs that match the DNA to be inserted.

**B)** During the uLoop assembly process, four DNA elements in the same level ($L_n$) are cut with the corresponding enzyme to make four linear DNA fragments. Since the Type IIS enzymes leave the inserts with matching overhangs that reflect their relative positions in the final assembled plasmid, these inserts only ligate in this specific alignment: insert1-insert2-insert3-insert4. The restriction enzyme also cuts out the *lacZ* gene from the next level ($L_{n+1}$) backbone and leaves overhangs for the final insert combination. The successfully assembled plasmid product includes the correct antibiotic selection gene for that level while excluding the *lacZ* gene. LB agar plates containing the appropriate antibiotic along with BluoGal+Isopropyl β-D-1-thiogalactopyranoside (IPTG) blue-white screening, which differentiate the colonies with wanted plasmid result (white) from the colonies with the unwanted backbone (blue), are used to select for assembled parts.

**C)** The overall assembly process follows this trend where SapI is used for making even level parts (L2 and L4) and BsaI is used for making odd level (L3) parts. The antibiotics selection markers are also separated in a similar way with KanR on the odd level plasmids and SpecR on the even level plasmids. The level of the plasmid also reflects the number of DNA elements in the plasmid.
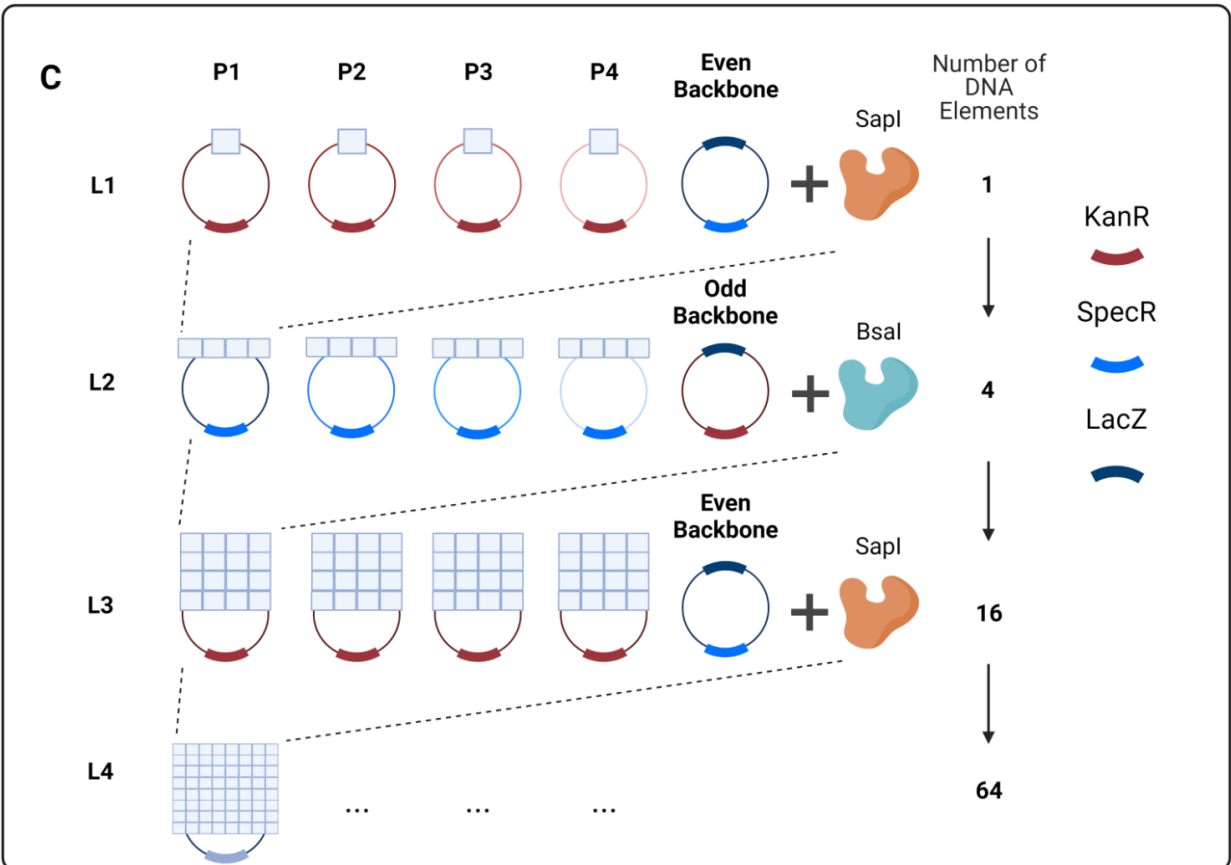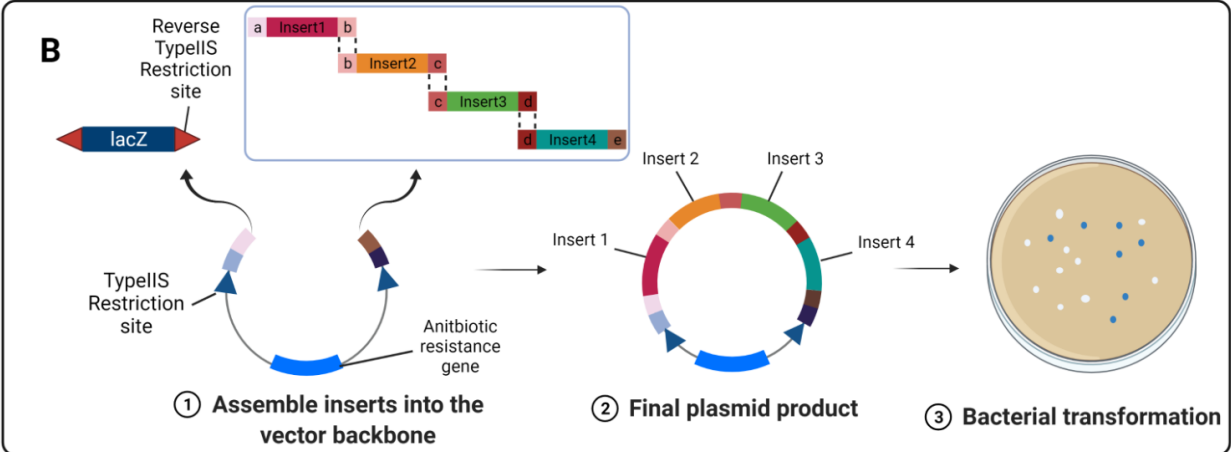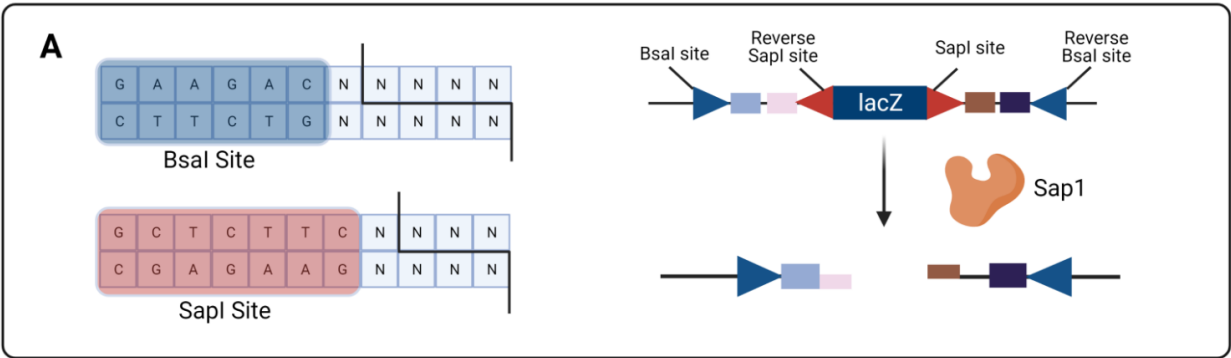
2.3.2 Bacterial Transformation with Electroporation

The bacterial transformations with uLoop assembled plasmids were done using electroporation. Electrocompetent cells used in this process were derived from the 10-beta Electrocompetent *E. coli.* strain. For each assembled reaction, one vial of 30µL electrocompetent cell is thawed on ice and then mixed with 0.5 µL of loop assembly plasmid. In the meantime, one 1mm electroporation cuvette is pre-cooled on ice. The uLoop assembly reaction mixed with competent cells is transferred into the cold cuvettes for electroporation. Immediately after electroporation, 100 µL of SOC media is added into the cuvette, mixed, and then transferred into a 1.7 ml microcentrifuge tube. Electroporated cells are then incubated shaking at 37 ℃ for 1 hour to permit expression of the antibiotic genes prior to plating on selective media. After the incubation, the mixture is spread on the IPTG-added LB antibiotic plate to allow colonies to grow overnight at 37 ℃.

2.3.3 Miniprep DNA Purification

Select colonies are inoculated into culture tubes with 2.5 mL of Terrific Broth containing antibiotics. This process often takes 16 hours with 37℃ incubation. After the incubation, glycerol stocks were prepared with 750ml of liquid culture and 750ml 50% glycerol and frozen at -80C for long-term storage. The rest of the culture product is purified using a standard miniprep protocol to generate purified DNA plasmids for analysis.

Chapter 2 is co-authored with Kyriakakis, Phillip, and Coleman, Todd P. The thesis author was the primary author of this chapter.

**CHAPTER 3: LENSLESS IMAGING SETUP FOR NEURAL TRACING**

3.1 Background

Lensless imaging is an emerging technique in the field of optical imaging and microscopy. In the most commonly used epifluorescent microscope setup, the sample/specimen is illuminated with a light source, the light is absorbed by a fluorophore and then emitted as a longer wavelength. Both the light source and the emitted light passes through an objective that is focused on a small region of the sample. However, unlike these microscopes, lensless-based imaging systems collect light without an objective, allowing light collection from a larger sample area essentially the size of the optical sensor. This light pattern is recorded and then processed by precalibrated computational algorithms to reconstruct the original image[31].

In recent years, different approaches to achieve the lensless imaging have been developed including shadow imaging (placing the transmissive sample directly on top of the imaging sensor to minimize random diffraction) and mask-based imaging (a mircofabric phase mask is used in front of the sensor to cause known diffraction patterns that can allow calculation of the light coming from the sample to reconstruct the image)[30,44]. Since many approaches have adopted this concept, these lensless imaging techniques are capable of acquiring images with a significantly larger field-of-view (FOV) compared to conventional microscopes while maintaining a reasonable spatial resolution[45]. This larger FOV makes lensless imaging techniques capable of imaging the large areas of an entire mouse or rat brain slice, which can be used for more rapid and trans-synaptic neuronal tracing.

For *in vitro* and *in slice* neural tracing applications, traditional optogenetics methods are often paired with fluorescent microscopy for simultaneous imaging and optogenetic stimulation of neural activity to confirm functional synaptic connections. However, using a large

high-density LED panel for stimulation, coupled with a large high-density light sensor can achieve similar results at a much lower cost, a much lower footprint, and can all stay inside an incubator throughout the entire process. A lensless imaging system can be built with several orders of magnitude less cost with Complementary Metal-Oxide Semiconductor (CMOS) or Charge-Coupled Devices (CCD) for sensing and LEDs for illumination. In addition, combining the LEDs for genetic control of viral spread and light sensors for tracking the viral spread can enable automation of mapping specific polysynaptic connections. These advantages are well-suited for the viral vector neural tracing demonstrated in chapter 2. A framework to build such a system with commercially available electronics is discussed in this chapter.

## 3.2 Design of the Stimulation and Imaging System

Similar to the shadow imaging approach, the lensless imaging system developed in this work can be described as two complexes. The core components of these two complexes are a DSLR CMOS sensor for image capture and an Organic Light-Emitting Diode (OLED) light panel for illumination. As shown in the schematic diagram in **Figure 6**, the overall architecture starts with the illumination panel (OLED display) at the bottom of the device, a specimen chamber in the middle, and an imaging sensor on the top. The main purpose of this type of inverted setup compared to common shadow lensless imaging setups is to be able to place the sample as close to the OLEDs as possible to achieve precise activation of the optogenetics system. The specimen is placed directly on top of the OLED with each OLED pixel regulating output intensities and wavelength of the light at a specific region.

For the illumination system, LEDs/OLEDswere chosen because, unlike Liquid Crystal Displays (LCD), it does not require a backlight, minimizing heat and unwanted light leakage. Since the PhyB photoreceptor is highly sensitive to red light activation (saturating at

40nW/cm$^2$)[26]. For imaging, CMOS sensors are commonly used in lensless imaging. Compared to their counterpart, CCD sensors, CMOS sensors are better suited for lab-on-chip applications because of their faster digital readout speed and lower power consumption rate. In addition, the usage of a CMOS chip extracted from a DSLR camera is widely available and inexpensive. Using this design, sections of the rat's brain (20.7mm x 15.5 mm) or the mouse's brain (13.7mm x 5.5mm) can be used. The large active pixel area (~ 20mm x 20mm) of a standard DSLR CMOS sensor provides sufficient effective sensing to capture the entire cross-sectional area in one frame. However, several sensors could be easily combined and illumined using a larger LED panel (*e.g.* an iPAD) for imaging and tracing in larger brains.
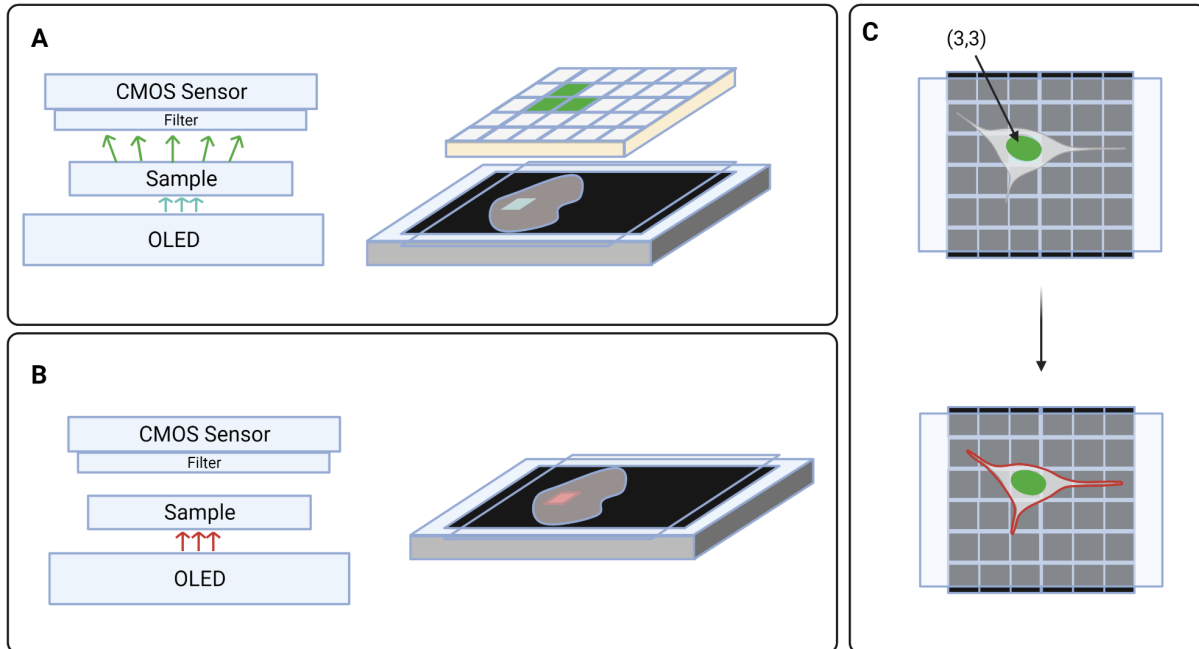
**Figure 6: Lensless imaging and optogenetic stimulation system using a CMOS sensor and OLED panel.**

**A)** The system architecture represents the horizontal relationship between the OLED panel, sample of interest, emission filter, and the CMOS sensor. Neurons initially infected with BV will produce nuclear GFP signals which can be detected by this setup.

**B)** Red pixels from the OLED panel will be used to activate the PhyB photoreceptor inducing *L* gene expression and RV spreading to neurons connected to the stimulated cell.

**C)** This setup viewed from the top shows how the single nuclei of a neuron can be stimulated by an OLED (pixel) to activate viral spreading and Cre recombination to label infected cells with high spatial accuracy.

## 3.3 Hardware Configuration

To design a system that can be affordable, scalable and off the shelf, the following commercially available components were chosen for this project:

**OLED light panel**

The illumination equipment used was the 1.27" OLED Breakout Board with 16-bit color control from Adafruit. This active display panel is made up of 128 x 96 RGB pixels with a 250μm x 250μm pixel size.

**CMOS sensor**

The CMOS sensor used was from a Canon EOS 10D, 6.3 megapixel DSLR, with an effective imaging area is 22.7mm x 15.1mm, and pixel pitch is 7.38 μm.

**Hardware control**

For the convenience of integrating post processing with computational algorithms in the future, all the electronics are communicated through a Windows Form-based application written for a PC system. This system was designed such that users can pass in defined parameters into microprocessors used to control the illumination pattern on the OLED and to forward commands to the DSLR camera CMOS sensor for image capturing, RAW image file extracting, and file transferring from DSLR to PC. In this project, the microprocessors used to achieve these features are an Arduino UNO board and a Raspberry Pi 4 for the OLED and DSLR respectively (**Figure 7**).
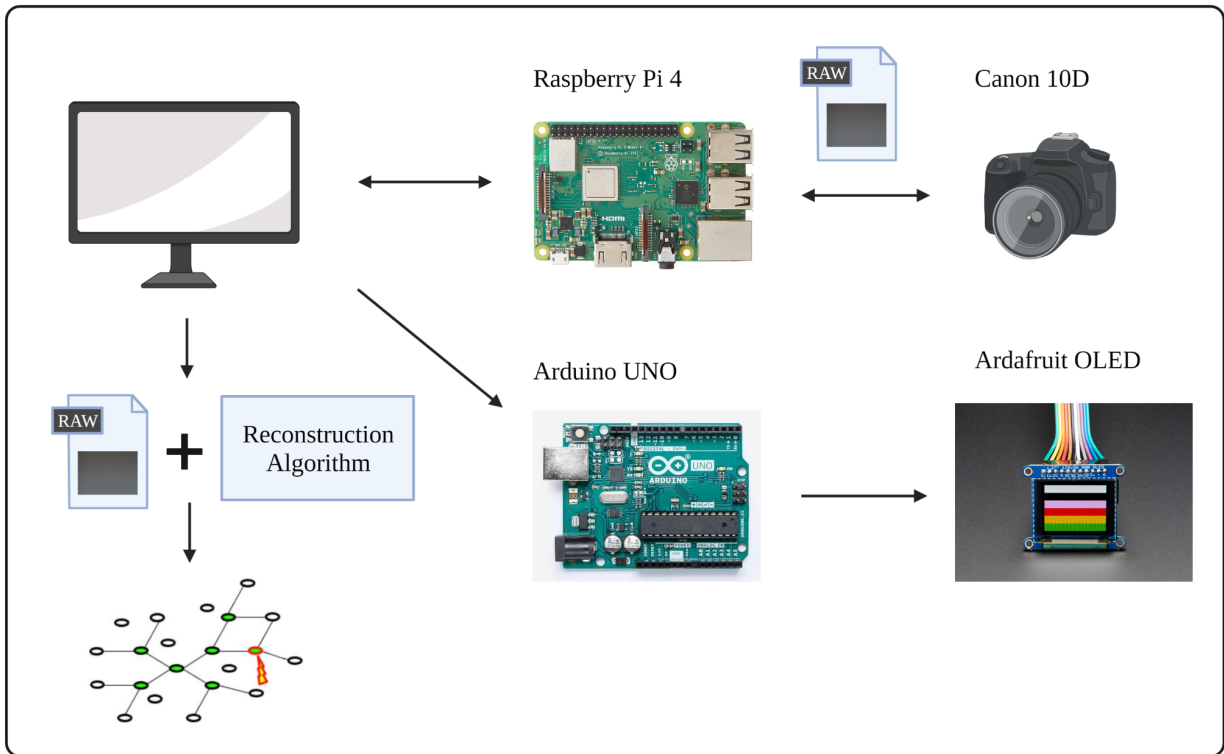
**Figure 7: Integrated configuration for controlled illumination and image acquisition.**

Raspberry Pi and Arduino UNO are the board-level processors connected to a DSLR camera CMOS sensor and the OLED screen respectively. Arrows indicate the directionality of signal transmissions. After triggering the capture function of the DSLR camera, the resulting image file is generated in the RAW format and then sent back to the PC for post processing and analysis.

3.4 Software Architecture and Protocol Establishment

To provide synchronous control over the hardware setup, software architecture and corresponding protocols were developed. As described in the hardware components section, the central controlling unit is the main User Interface (UI) application developed in the C# Windows Forms environment. General functions of this application include: initializing serial port communication for the Arduino Uno, loading illumination setting into Arduino Uno, passing user-defined time-lapse imaging parameters to Raspberry Pi, and file transfer from Raspberry Pi to the PC. For the simplicity of future modifications and expansions, independent communication protocols were written between the two microprocessors and the main controlling unit, a PC in this case. Following sections will explain these parts in detail.

3.4.1 Configuration of the Illumination Panel with the Arduino Uno

In this setup, digital strings that encode locational and wavelength information of the user-defined illumination pattern are streamed from PC to Arduino using a USB serial connection. The USB port used for this data transmission is initialized once the UI application starts. Then, the AD2OLED.ino script, uploaded and contained in the Arduino memory, will constantly scan and decipher valid serial inputs. The encoding and deciphering algorithm utilizes a relatively straightforward structure that compiles the information into specific character sequences (**Figure 8**). Since the OLED panel used in the setup has a resolution of 128 x 96, all geometrical shapes can be decomposed into a series of rectangles with x,y coordinates and corresponding widths and heights represented by 3 digits. Once this information is successfully extracted from the string, the Arduino Uno makes function calls with these parameters to display the programmed pattern. With this serial communication process, the light source can be configured precisely with millisecond precision for optogenetics applications.

29
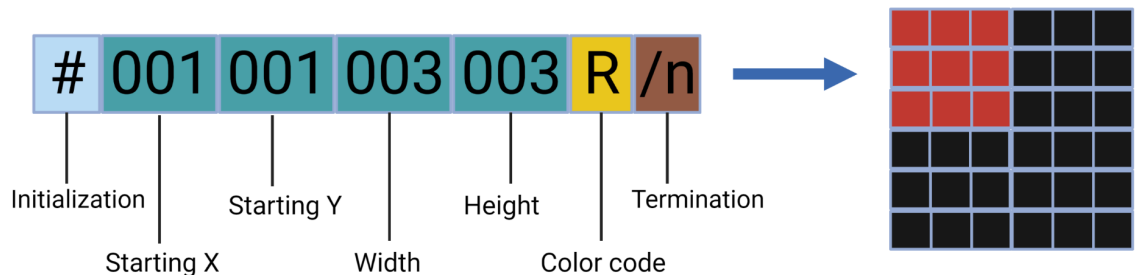
**Figure 8: Data structure encoded for OLED display information.**

3.4.2 Camera Control and File Transferring using the Raspberry Pi

To decrease latency in data transmission and increase the stability of the system, a two-way communication system between the PC and Raspberry Pi is established through an ethernet connection. The oversight and encryption of this ethernet connection are done from the PC side using the PuTTY Secure Shell Protocol (SSH) platform. Besides the actual PuTTY client itself, two packages are needed for this application: (1) plink, command line interface for remote execution of a python file on the Raspberry, and (2) pscp, SSH encrypted file transfer. The actual implementations of these two packages are done by specific event-handling scripts: PC2Pi_CC.py and PC2Pi_FT.py (CC stands for Camera Control and FT stands for File Transfer). Through the camera control script, time-lapsed imaging settings, such as the total number of shots and time interval in between shots, are parsed into the recipient script, ImageCapture.py, on the Raspberry Pi as input parameters. This recipient script adopted functions from the gphoto2 library to interface with the Canon 10D camera (gphoto2 supports digital access of many commercially available DSLR cameras). The final software architecture combined with all the protocols is shown in **Figure 9**. And the final main UI is shown in **Figure 10**. These files are available on GitHub https://github.com/BreakLiquid/Neural_Tracing.git. Chapter 3 is co-authored with Kyriakakis, Phillip, and Coleman, Todd P. The thesis author was the primary author of this chapter.
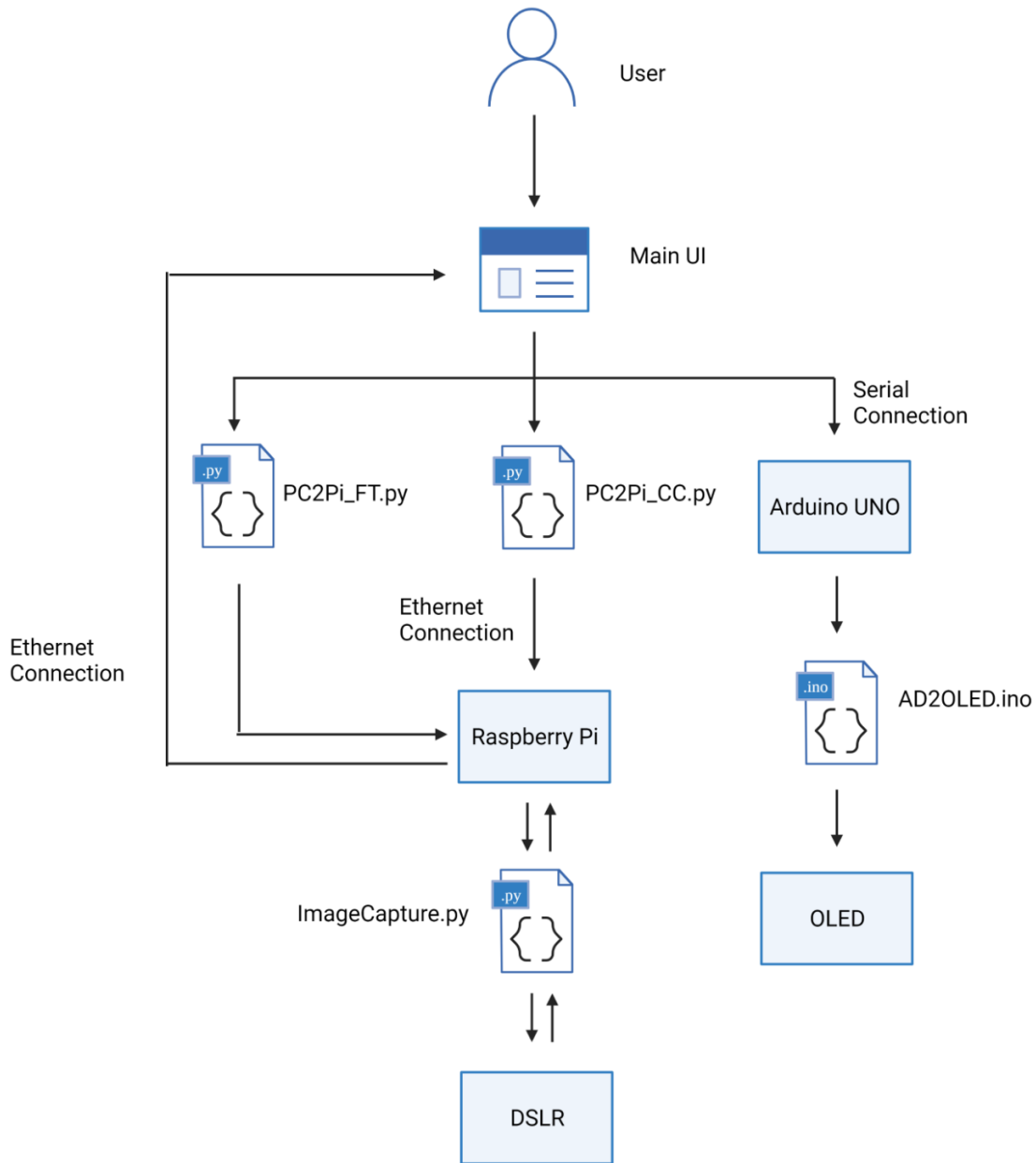
**Figure 9: Overview of the software architecture.**

Functions like generating the desired illumination on the OLED panel, capturing images with DSLR, and transferring image files from Raspberry Pi to PC are initialized at the main UI. For the OLED control, the user inputs will be converted into an information encoded string and sent to the Arduino UNO through the serial I/O. A pre-loaded Arduino script will decipher the input string and output corresponding pattern alteration. For camera capture (CC) and file transfer (FT), an ethernet connection is used.
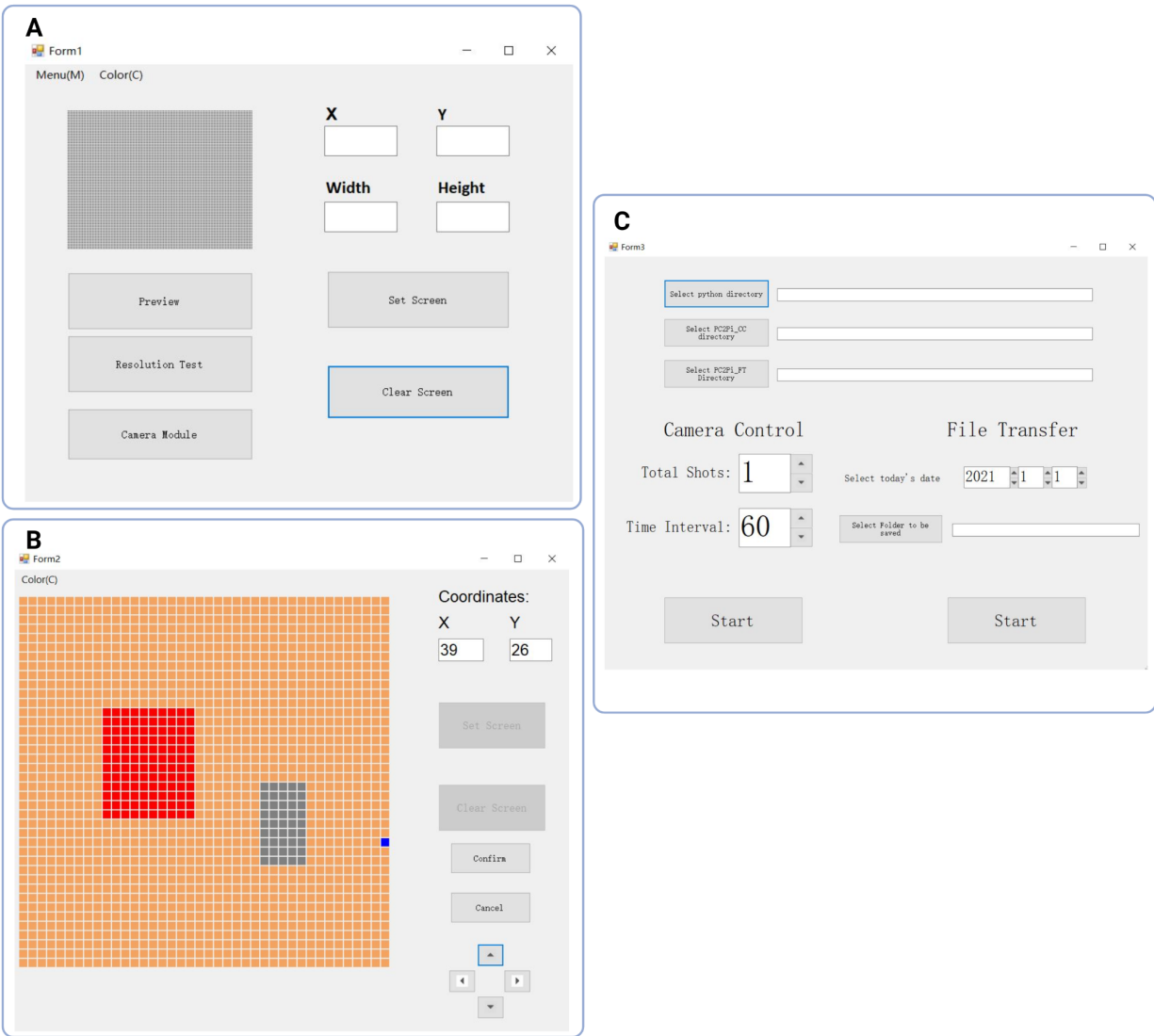
**Figure 10: The user interface of the main application.**

**A)** This is the initial form that will be shown once the application is opened. The pixelated map on the top-left represents the current display of the panel. Digital inputs on the right allow some basic configurations of the OLED. This form also provides options such as resolution testing and clear screen. From this window, users can also open the other two forms. "Preview" button leads to Form2 and the "Camera Module" leads to Form3.

**B)** The canvas on the right is the map for pixel selection which can be done by a click and drag motion of the cursor. The current cursor location is highlighted in blue and its coordinates are displayed on the top-right corner. The red region represents the active pixel area. The grey region represents the area selected, but not yet active. Users can navigate through different sections of this panel using the arrow keys.

**C)** This form sets up the parameters for image capturing and transferring. Since all the image files saved on the Raspberry Pi are labeled by the time the image was taken, the transferring process requires the time information to locate the files.

**CHAPTER 4: CONCLUSION**

Constructing the expression plasmids for the baculovirus neural tracer with PhyB optogenetic control of viral spreading and developing synchronized lensless imaging setup from commercially available sensors and light sources were the two main components of this work. Brief summaries of each part of the project and possible future directions are discussed in the following section.

4.1 Summary of the Construction on Optically Controlled Viral Neural Tracer

A light-sensitive viral neuronal tracing system that is capable of selective labeling of long-range polysynaptic connections with limited cytotoxicity was designed based on the properties of the double-deletion rabies virus RVΔGL-Cre[35]. Since the RVΔGL-Cre has genes essential for allowing them to replicate and spread from one neuron to another deleted, these genes must be complemented or replaced to rescue these functions. To achieve this, the BV was chosen as the helper virus to deliver necessary complementary proteins. In the end, the functional components the BV will deliver include: the PhyB/PIF3 gene switch for optical control of *L* gene expression, a Cre-dependent reporter for differential neuron labeling, and TVA+G proteins for neuron transduction and spreading by RVΔGL-Cre. The resulting baculovirus expression cassettes (PhyB-Lgene, PhyB-destableLgene, positive control) were constructed in bacterial plasmids so that they can be transferred and inserted into the BV genome through Tn7-mediated transposition. In order to efficiently clone and validate these plasmid constructs, the uLoop DNA assembly was used. The final plasmid products have sizes 29.4kb for PhyB-Lgene and PhyB-destableLgene, and 17.8 kb for Lgene-PositiveCtrl. Because of the recursive assembly process of uLoop, the final level 4 plasmid constructs were made out of four level 3 plasmid parts which themselves were made from lower level parts. Therefore, the plasmids containing all

the functional DNA elements used in this project (for example PhyB/PIF3 vector, *L* gene, *G* gene, TVA gene, insulators, and other expression-related modulators) were established and can be used to assemble many other versions of this system.

## 4.2 Summary of the Development for Lensless Imaging Setup

In the lensless imaging setup, the two main functional units, the illumination system, and the imaging sensor were composed of a commercially available OLED panel and DSLR CMOS chip. In order to synchronously control both hardware devices, a software framework that connects the OLED panel and CMOS sensor with their corresponding microcontrollers, Arduino and Raspberry Pi, was constructed. With specified communication protocols, the end user can pass on commands such as triggering time-lapse imaging and changing displays with a user-friendly interface built on a PC platform. The image file transfer between the sensor module to the PC had also been protected with secure shell protocol. When applied to viral vector tracing, this setup will allow users to modify the illumination display for spatially specific activation of the optogenetics switches (controlling viral spreading, any gene of interest or neural activity) in real-time without the need of taking out the neuron samples in and out of their incubation environment or a microscope.

## 4.3 Future Directions

For the viral vector design portion of this work, there are a few *in vitro* experiments that can be done with the three expression cassettes in the future to further optimize and validate the concept of using BV as the helper virus for the RVΔGL-Cre. Since the cassettes are currently placed within the bacterial plasmids, the first step will be to transpose the DNA inserts into the Baculovirus receiver vectors using the BAC-to-Bac system. The resulting BV vectors would then be purified and transfected into insect cells (Sf9) to produce functional BVs carrying the

designed cassettes. With these BVs, the next step will be to test them in actual cultured neurons or mouse brain slices. First, the positive control BV can be used to test rescue the RVΔGL-Cre, independent of light using cultured neurons or slices. Then, to test the light control of spreading, neurons can be separated into two groups with both of them first infected with PhyB-Lgene BV and then infected with RVΔGL-Cre (Since the BV contains the TVA receptor for RV infection, this process must be sequential, though transgenic mice expressing TVA could circumvent that need). Then one group will receive red light activation and the other will be kept in the dark. The resulting distribution of mScalert-CAAX reporters, which indicates RV trans-neural spreading should only appear in the sample that has been illuminated with red light. Next, the concept of spatially controlling the spread of RV can be tested. Since PhyB optogenetic control of cellular activity has been done on a subcellular level in the previous studies, single-cell control of transsynaptic spreading should be feasible[46,47]. Another important consideration with the BV construct is to limit cytotoxicity. Control experiments can be set up with different varying parameters such as *L* gene vs destabilized *L* gene, different pulse lengths for the red light activation, and different pulse frequencies. This level of control, both on *L* gene levels and on a single cell level has not yet been achieved and the PhyB gene control system can enable the level of control to find the amount of activation needed for spreading. Moreover, since the PhyB system can be shut off with far-red light, the *L* gene can be minimally expressed, minimizing cellular toxicity in a way never before possible. Future directions for the lensless imaging setup would be to calibrate the parameters associated with the neural tracing applications such as intensity of the illumination, and filter choices. After these related parameters are defined, a stable structure that fits the requirements should be used to confine the hardware to ensure repeatable stimulation and imaging results. For post-imaging analysis, there is still a need to

develop the image reconstruction algorithm that fits well with the fluorescent signal of the neuron sample. Since the signal used to target the neuron is confined to the nucleus and the stimulation is only required in the nucleus, this level of precision should be achievable. One promising method is to use a Point-Spread-Function (PSF) estimation on the light source and deconvolve the raw image into useful information. This method has been applied in numerous lensless imaging applications achieving robust reconstruction results. This conceptual design could be adapted using higher resolution LEDs with larger panels and combining multiple CMOS sensors to trace larger brain slices or multiple brain slices on a single setup. Further, many of these devices can easily fit into a standard cell culture incubator, allowing mapping sections of entire brains or multiple brains.

# REFERENCES

1.      Lerner TN, Ye L, Deisseroth K. Communication in Neural Circuits: Tools, Opportunities, and Challenges. Cell. 2016 Mar 10;164(6):1136-1150. doi: 10.1016/j.cell.2016.02.027. PMID: 26967281; PMCID: PMC5725393.

2.      Rubinov M, Bullmore E. Fledgling pathoconnectomics of psychiatric disorders. Trends Cogn Sci. 2013 Dec;17(12):641-7. doi: 10.1016/j.tics.2013.10.007. Epub 2013 Nov 15. PMID: 24238779.

3.      Oztas, Emin. "Neuronal tracing." Neuroanatomy 2.2 (2003): 5.

4.      Lanciego JL, Wouterlood FG. A half century of experimental neuroanatomical tracing. J Chem Neuroanat. 2011 Nov;42(3):157-83. doi: 10.1016/j.jchemneu.2011.07.001. Epub 2011 Jul 18. PMID: 21782932.

5.      Kristensson K, Olsson Y. Retrograde axonal transport of protein. Brain Res. 1971 Jun 18;29(2):363-5. doi: 10.1016/0006-8993(71)90044-8. PMID: 4107258.

6.      Saleeba C, Dempsey B, Le S, Goodchild A, McMullan S. A Student's Guide to Neural Circuit Tracing. Front Neurosci. 2019 Aug 27;13:897. doi: 10.3389/fnins.2019.00897. Erratum in: Front Neurosci. 2020 Mar 10;14:177. PMID: 31507369; PMCID: PMC6718611.

7.      Grafstein B. Transport of protein by goldfish optic nerve fibers. Science. 1967 Jul 14;157(3785):196-8. doi: 10.1126/science.157.3785.196. PMID: 6029096.

8.      Köbbert C, Apps R, Bechmann I, Lanciego JL, Mey J, Thanos S. Current concepts in neuroanatomical tracing. Prog Neurobiol. 2000 Nov;62(4):327-51. doi: 10.1016/s0301-0082(00)00019-8. PMID: 10856608.

9.      Vercelli A, Repici M, Garbossa D, Grimaldi A. Recent techniques for tracing pathways in the central nervous system of developing and adult mammals. Brain Res Bull. 2000 Jan 1;51(1):11-28. doi: 10.1016/s0361-9230(99)00229-4. PMID: 10654576.

10.     Goshgarian HG, Buttry JL. The pattern and extent of retrograde transsynaptic transport of WGA-Alexa 488 in the phrenic motor system is dependent upon the site of application. J Neurosci Methods. 2014 Jan 30;222:156-64. doi: 10.1016/j.jneumeth.2013.11.003. Epub 2013 Nov 12. PMID: 24239778; PMCID: PMC4068738.

11.     Duarte MJ, Kanumuri VV, Landegger LD, Tarabichi O, Sinha S, Meng X, Hight AE, Kozin ED, Stankovic KM, Brown MC, Lee DJ. Ancestral Adeno-Associated Virus Vector Delivery of Opsins to Spiral Ganglion Neurons: Implications for Optogenetic Cochlear Implants. Mol Ther. 2018 Aug 1;26(8):1931-1939. doi:

10.1016/j.ymthe.2018.05.023. Epub 2018 Jul 13. PMID: 30017876; PMCID: PMC6094394.

12.   Martell JD, Deerinck TJ, Lam SS, Ellisman MH, Ting AY. Electron microscopy using the genetically encoded APEX2 tag in cultured mammalian cells. Nat Protoc. 2017 Sep;12(9):1792-1816. doi: 10.1038/nprot.2017.065. Epub 2017 Aug 10. PMID: 28796234; PMCID: PMC5851282.

13.   Luo L, Callaway EM, Svoboda K. Genetic Dissection of Neural Circuits: A Decade of Progress. Neuron. 2018 Apr 18;98(2):256-281. doi: 10.1016/j.neuron.2018.03.040. Erratum in: Neuron. 2018 May 16;98 (4):865. PMID: 29673479; PMCID: PMC5912347.

14.   Holehonnur R, Lella SK, Ho A, Luong JA, Ploski JE. The production of viral vectors designed to express large and difficult to express transgenes within neurons. Mol Brain. 2015 Feb 24;8:12. doi: 10.1186/s13041-015-0100-7. PMID: 25887710; PMCID: PMC4359567.

15.   Ugolini G. Rabies virus as a transneuronal tracer of neuronal connections. Adv Virus Res. 2011;79:165-202. doi: 10.1016/B978-0-12-387040-7.00010-X. PMID: 21601048.

16.   Wickersham IR, Finke S, Conzelmann KK, Callaway EM. Retrograde neuronal tracing with a deletion-mutant rabies virus. Nat Methods. 2007 Jan;4(1):47-9. doi: 10.1038/nmeth999. Epub 2006 Dec 10. PMID: 17179932; PMCID: PMC2755236.

17.   Duebel J, Marazova K, Sahel JA. Optogenetics. Curr Opin Ophthalmol. 2015 May;26(3):226-32. doi: 10.1097/ICU.0000000000000140. PMID: 25759964; PMCID: PMC5395664.

18.   Hartmann D, Smith JM, Mazzotti G, Chowdhry R, Booth MJ. Controlling gene expression with light: a multidisciplinary endeavour. Biochem Soc Trans. 2020 Aug 28;48(4):1645-1659. doi: 10.1042/BST20200014. PMID: 32657338; PMCID: PMC7458398.

19.   Kyriakakis P, Catanho M, Hoffner N, Thavarajah W, Hu VJ, Chao SS, Hsu A, Pham V, Naghavian L, Dozier LE, Patrick GN, Coleman TP. Biosynthesis of Orthogonal Molecules Using Ferredoxin and Ferredoxin-NADP+ Reductase Systems Enables Genetically Encoded PhyB Optogenetics. ACS Synth Biol. 2018 Feb 16;7(2):706-717. doi: 10.1021/acssynbio.7b00413. Epub 2018 Jan 24. PMID: 29301067; PMCID: PMC5820651.

20.   Kyriakakis P, Fernandez de Cossio L, Howard PW, Kouv S, Catanho M, Hu VJ, Kyriakakis R, Allen ME, Ma Y, Aguilar-Rivera M, Coleman TP. Building a Simple and Versatile Illumination System for Optogenetic Experiments. J Vis Exp. 2021 Jan 12;(167). doi: 10.3791/61914. PMID: 33522514.

21.    Pathak GP, Strickland D, Vrana JD, Tucker CL. Benchmarking of optical dimerizer systems. ACS Synth Biol. 2014 Nov 21;3(11):832-8. doi: 10.1021/sb500291r. Epub 2014 Nov 5. PMID: 25350266; PMCID: PMC4277767.

22.    Tabor JJ, Levskaya A, Voigt CA. Multichromatic control of gene expression in Escherichia coli. J Mol Biol. 2011 Jan 14;405(2):315-24. doi: 10.1016/j.jmb.2010.10.038. Epub 2010 Oct 28. PMID: 21035461; PMCID: PMC3053042.

23.    Ramakrishnan P, Tabor JJ. Repurposing Synechocystis PCC6803 UirS-UirR as a UV-Violet/Green Photoreversible Transcriptional Regulatory Tool in E. coli. ACS Synth Biol. 2016 Jul 15;5(7):733-40. doi: 10.1021/acssynbio.6b00068. Epub 2016 May 11. PMID: 27120220.

24.    Müller K, Engesser R, Metzger S, Schulz S, Kämpf MM, Busacker M, Steinberg T, Tomakidi P, Ehrbar M, Nagy F, Timmer J, Zubriggen MD, Weber W. A red/far-red light-responsive bi-stable toggle switch to control gene expression in mammalian cells. Nucleic Acids Res. 2013 Apr;41(7):e77. doi: 10.1093/nar/gkt002. Epub 2013 Jan 25. PMID: 23355611; PMCID: PMC3627562.

25.    QUAIL, P.H. (1997), An emerging molecular map of the phytochromes. Plant, Cell & Environment, 20: 657-665. https://doi.org/10.1046/j.1365-3040.1997.d01-108.x

26.    Shimizu-Sato S, Huq E, Tepperman JM, Quail PH. A light-switchable gene promoter system. Nat Biotechnol. 2002 Oct;20(10):1041-4. doi: 10.1038/nbt734. Epub 2002 Sep 3. PMID: 12219076.

27.    Gomez EJ, Gerhardt K, Judd J, Tabor JJ, Suh J. Light-Activated Nuclear Translocation of Adeno-Associated Virus Nanoparticles Using Phytochrome B for Enhanced, Tunable, and Spatially Programmable Gene Delivery. ACS Nano. 2016 Jan 26;10(1):225-37. doi: 10.1021/acsnano.5b05558. Epub 2015 Nov 30. PMID: 26618393.

28.    Mohanty SK, Lakshminarayananan V. Optical Techniques in Optogenetics. J Mod Opt. 2015;62(12):949-970. doi: 10.1080/09500340.2015.1010620. PMID: 26412943; PMCID: PMC4582796.

29.    Ojha A, Banik S, Melanthota SK, Mazumder N. Light emitting diode (LED) based fluorescence microscopy for tuberculosis detection: a review. Lasers Med Sci. 2020 Aug;35(6):1431-1437. doi: 10.1007/s10103-019-02947-6. Epub 2020 Jan 3. PMID: 31900690.

30.    Stark E, Koos T, Buzsáki G. Diode probes for spatiotemporal optical control of multiple neurons in freely moving animals. J Neurophysiol. 2012 Jul;108(1):349-63. doi: 10.1152/jn.00153.2012. Epub 2012 Apr 11. PMID: 22496529; PMCID: PMC3434617.

31. Ozcan A, McLeod E. Lensless Imaging and Sensing. Annu Rev Biomed Eng. 2016 Jul 11;18:77-102. doi: 10.1146/annurev-bioeng-092515-010849. Epub 2016 Jan 25. PMID: 27420569.

32. Ugolini G. Specificity of rabies virus as a transneuronal tracer of motor networks: transfer from hypoglossal motoneurons to connected second-order and higher order central nervous system cell groups. J Comp Neurol. 1995 Jun 5;356(3):457-80. doi: 10.1002/cne.903560312. PMID: 7642806.

33. Etessami R, Conzelmann KK, Fadai-Ghotbi B, Natelson B, Tsiang H, Ceccaldi PE. Spread and pathogenic characteristics of a G-deficient rabies virus recombinant: an in vitro and in vivo study. J Gen Virol. 2000 Sep;81(Pt 9):2147-2153. doi: 10.1099/0022-1317-81-9-2147. PMID: 10950970.

34. Liu YJ, Ehrengruber MU, Negwer M, Shao HJ, Cetin AH, Lyon DC. Tracing inputs to inhibitory or excitatory neurons of mouse and cat visual cortex with a targeted rabies virus. Curr Biol. 2013 Sep 23;23(18):1746-55. doi: 10.1016/j.cub.2013.07.033. Epub 2013 Aug 29. PMID: 23993841; PMCID: PMC3786040.

35. Chatterjee S, Sullivan HA, MacLennan BJ, Xu R, Hou Y, Lavin TK, Lea NE, Michalski JE, Babcock KR, Dietrich S, Matthews GA, Beyeler A, Calhoon GG, Glober G, Whitesell JD, Yao S, Cetin A, Harris JA, Zeng H, Tye KM, Reid RC, Wickersham IR. Nontoxic, double-deletion-mutant rabies viral vectors for retrograde targeting of projection neurons. Nat Neurosci. 2018 Apr;21(4):638-646. doi: 10.1038/s41593-018-0091-7. Epub 2018 Mar 5. PMID: 29507411; PMCID: PMC6503322.

36. Nakagawa K, Kobayashi Y, Ito N, Suzuki Y, Okada K, Makino M, Goto H, Takahashi T, Sugiyama M. Molecular Function Analysis of Rabies Virus RNA Polymerase L Protein by Using an L Gene-Deficient Virus. J Virol. 2017 Sep 27;91(20):e00826-17. doi: 10.1128/JVI.00826-17. PMID: 28768857; PMCID: PMC5625484.

37. Naik NG, Lo YW, Wu TY, Lin CC, Kuo SC, Chao YC. Baculovirus as an efficient vector for gene delivery into mosquitoes. Sci Rep. 2018 Dec 12;8(1):17778. doi: 10.1038/s41598-018-35463-8. PMID: 30542209; PMCID: PMC6290771.

38. Molinari P, Molina GN, Tavarone E, Del Médico Zajac MP, Morón G, Taboga O. Baculovirus capsid display in vaccination schemes: effect of a previous immunity against the vector on the cytotoxic response to delivered antigens. Appl Microbiol Biotechnol. 2018 Dec;102(23):10139-10146. doi: 10.1007/s00253-018-9368-8. Epub 2018 Sep 20. PMID: 30238142.

39. Hancock JF, Cadwallader K, Paterson H, Marshall CJ. A CAAX or a CAAL motif and a second signal are sufficient for plasma membrane targeting of ras proteins. EMBO J. 1991 Dec;10(13):4033-9. PMID: 1756714; PMCID: PMC453151.

40.     Airenne KJ, Peltomaa E, Hytönen VP, Laitinen OH, Ylä-Herttuala S. Improved generation of recombinant baculovirus genomes in Escherichia coli. Nucleic Acids Res. 2003 Sep 1;31(17):e101. doi: 10.1093/nar/gng102. PMID: 12930975; PMCID: PMC212821.

41.     Loetscher P, Pratt G, Rechsteiner M. The C terminus of mouse ornithine decarboxylase confers rapid degradation on dihydrofolate reductase. Support for the pest hypothesis. J Biol Chem. 1991 Jun 15;266(17):11213-20. PMID: 2040628.

42.     Engler C, Marillonnet S. Golden Gate cloning. Methods Mol Biol. 2014;1116:119-31. doi: 10.1007/978-1-62703-764-8_9. PMID: 24395361.

43.     Pollak B, Matute T, Nuñez I, Cerda A, Lopez C, Vargas V, Kan A, Bielinski V, von Dassow P, Dupont CL, Federici F. Universal loop assembly: open, efficient and cross-kingdom DNA fabrication. Synth Biol (Oxf). 2020;5(1):ysaa001. doi: 10.1093/synbio/ysaa001. Epub 2020 Feb 5. PMID: 32161816; PMCID: PMC7052795.

44.     G. Kuo, N. Antipa, R. Ng, and L. Waller, DiffuserCam: Diffuser-Based Lensless Cameras. Imaging and Applied Optics 2017 (3D, AIO, COSI, IS, MATH, pcAOP), OSA Technical Digest (online) (Optical Society of America, 2017), paper CTu3B.2.

45.     Bishara W, Su TW, Coskun AF, Ozcan A. Lensfree on-chip microscopy over a wide field-of-view using pixel super-resolution. Opt Express. 2010 May 24;18(11):11181-91. doi: 10.1364/OE.18.011181. PMID: 20588977; PMCID: PMC2898729.

46.     Levskaya A, Weiner OD, Lim WA, Voigt CA. Spatiotemporal control of cell signalling using a light-switchable protein interaction. Nature. 2009 Oct 15;461(7266):997-1001. doi: 10.1038/nature08446. Epub 2009 Sep 13. PMID: 19749742; PMCID: PMC2989900.

47.     Adrian M, Nijenhuis W, Hoogstraaten RI, Willems J, Kapitein LC. A Phytochrome-Derived Photoswitch for Intracellular Transport. ACS Synth Biol. 2017 Jul 21;6(7):1248-1256. doi: 10.1021/acssynbio.6b00333. Epub 2017 Mar 30. PMID: 28340532; PMCID: PMC5525101.